K Auger rates calculated for Ne^+*

Hugh P. Kelly
Department of Physics, University of Virginia, Charlottesville, Virginia 22901
(Received 30 September 1974)

Starting with a $1s$ vacancy in the neon atom, Auger rates are calculated for transitions to the final LS-coupled states of Ne^{++}. Electron correlations are found to have a significant effect on these rates. Although the configuration mixing of Ne^{++} $(1s)^2(2s)^2(2p)^4\ ^1S$ and $(1s)^2(2p)^6\ ^1S$ is important, good results are only obtained by also considering the other correlation effects representing mixing with other configurations. The ratios of calculated Auger rates relative to the $1s$-$2s2s\ ^1S$ rate are in close agreement with experiment. However, the calculated absolute rates are all higher than the experimental values of Mehlhorn, Stalherm, and Verbeek by factors ranging from 1.4 to 1.5.

I. INTRODUCTION

Recently there has been considerable interest in studying the Auger electrons emitted in heavy particle collisions with neon.[1-3] The positions and intensities of the many resulting Auger lines reveal much information about the initial collision. Theoretical calculations[4,5] carried out for many different initial vacancy configurations can be of considerable aid in understanding the experimental data. In such calculations it is important to be able to estimate the accuracy of the calculated results; and it is desirable, therefore, to be able to carry out calculations which agree with known experimental data.

Reviews of Auger-effect experiments and calculations have been given by Bambynek *et al.*[6] and by Burhop and Asaad.[7] As discussed by Burhop and Asaad,[7] for light elements relative intensities calculated theoretically are in poor agreement with the experimental results. Recently, Bhalla has calculated the relative intensities of the KLL lines of Ne using Hartree-Slater orbitals and including configuration mixing between the final Ne^{++} states, $1s^22p^6\ ^1S$ and $1s^22s^22p^4\ ^1S$. The importance of including the mixing of these two configurations was first pointed out by Asaad[8] who found that inclusion of this mixing considerably improved the agreement between theory and experiment of elements of Z ranging from 12 to 36. For Ne when LS coupling is used, there are five different lines corresponding to final states: $(1s)^2(2p)^6\ ^1S$, $(1s)^2(2s)(2p)^5\ ^1P$, $(1s)^2(2s)(2p)^5\ ^3P$, $(1s)^2(2s)^2(2p)^4\ ^1S$, and $(1s)^2(2s)^2(2p)^4\ ^1D$. The configuration mixing of $(1s)^2(2p)^6\ ^1S$ and $(1s)^2(2s)^2(2p)^4\ ^1S$ can only directly affect the intensities of these two lines. In calculating the ratios of the intensities for the other four lines to the $1s^22p^6\ ^1S$ line, Bhalla[9] found considerable improvement over the direct Hartree-Slater results when this configuration mixing was included. However, the ratio of the $(1s)^2(2s)^2(2p)^4\ ^1S$ intensity to that of $(1s)^2(2p)^6\ ^1S$ was still found to be rather poor, being 0.99 as compared with 1.55 and 1.5 from two different experiments.[10,11] Also, Bhalla[9] did not report absolute intensities, although absolute intensities had been measured for all five lines in the interesting experiment of Mehlhorn, Stalherm, and Verbeek.[10]

In this work the absolute intensities are calculated for all five lines, first using the Hartree-Fock approximation and then including correlation effects by use of many-body perturbation theory.[12-14] We have used LS coupling and neglected spin-orbit effects. In a previous paper[15] we have discussed the use of many-body theory for calculating Auger rates. The total K Auger rate for Ne^+ was calculated to lowest order (essentially in the Hartree-Fock approximation), and a rough estimate of some higher-order terms was given. However, as shown in this paper, the treatment of the higher-order terms was not adequate. Also, the previous work did not specifically list the separate contributions to the five distinct lines in LS coupling. In this paper these deficiencies are corrected, and comparison is made with the experimental results of Mehlhorn *et al.*[10]

II. THEORY

In Ref. 15 it was shown that the Auger rate is proportional to the imaginary part of the energy when only Coulomb interactions are included and denominators D are replaced by $D+i\eta$, where $\eta \to 0$. The denominators are treated according to

$$(D+i\eta)^{-1} = PD^{-1} - i\pi\delta(D), \tag{1}$$

where P represents principal-value integration. In calculating the Auger rate by diagrammatic perturbation theory,[12-14] we may either calculate the imaginary parts of all energy diagrams for Ne^+ with a $1s$ vacancy or we may calculate the diagrams for the Auger transition matrix elements. These diagrams are obtained by separating the energy

diagrams into two parts where a vanishing denominator is treated according to the $-i\pi\delta(D)$ of Eq. (1). We then consider only that part of the energy diagram which is either above or below the singularity. The total Auger rate is proportional to the absolute square of the sum of the matrix element diagrams. There are, however, small normalization corrections[14] which are treated separately. This treatment is completely analogous to that for obtaining photoionization cross sections where we consider the sum of "open" diagrams contributing to the many-particle transition matrix element from the initial state to the continuum.[16]

In Fig. 1 are shown the diagrams corresponding to the two lowest orders of perturbation theory. Note that certain exchange diagrams have not been explicitly drawn. For example, in Fig. 1(d) the bottom matrix element $\langle 1sk'|v|pr\rangle$ may be replaced by $\langle k'1s|v|pr\rangle$. To obtain a given many-particle Auger matrix element, one can project the determinantal state corresponding to a given diagram onto the given final (LS-coupled) many-particle state. Alternatively, one can calculate the many-particle Auger matrix element in the Hartree-Fock (HF) approximation, obtaining a linear combination of Coulomb matrix elements involving single-particle orbitals. Corrections to these Coulomb matrix elements are obtained by calculating the higher-order diagrams which have the same external hole and particle lines as the first-order Coulomb (HF) matrix elements. The diagrams are essentially equivalent to configuration mixing by Rayleigh-Schrödinger perturbation theory. We interpret diagrams (b), (c), (d), and (i) as corresponding to configuration mixing (or correlations) in the final state where the initial $1s$ vacancy is filled. Diagrams (e), (f), (g), and (h) correspond to configuration mixing in the initial state where there is a $1s$ vacancy.

III. RESULTS

The numerical calculations of this paper were carried out using the methods described in Refs. 14 and 15. In calculating matrix elements such as $\langle 1sk|v|pq\rangle$ of Fig. 1(a), the orbitals $1s$ and k were calculated with the configuration of the final state and orbitals p and q were calculated with the configuration of the initial state. In this way, some of the higher-order diagrams of perturbation theory are approximately included. In a few cases, the accuracy of this procedure was verified by calculating the higher-order diagrams starting with a complete orthogonal set of single-particle states corresponding to the initial state, $1s(2s)^2(2p)^6\ ^2S$. The final-state continuum orbital k was orthogonalized to the other orbitals of the same symmetry but this effect was found to be rather small. Also, there were only small changes in the matrix elements when the initial-state $1s$ orbital was used rather than the $1s$ orbital of the final state. The overlap matrix element $\langle 2pf|2pi\rangle$, where $2pi$ is the HF $2p$ orbital of the initial configuration $1s(2s)^2(2p)^6$ and $2pf$ is the HF $2p$ orbital of the final configuration $(1s)^2(2p)^6$, is 0.999286. Although the overlap factor of the full matrix element involves $(\langle 2pf|2pi\rangle)^6$, this is still a small effect.

A. Auger energies

The energy of the ejected electron $\epsilon_k = \frac{1}{2}k^2$ and is determined by

$$E_i = E_f + \tfrac{1}{2}k^2, \tag{2}$$

where E_i is the energy of the initial state $1s(2s)^2(2p)^6\ ^2S$ and E_f is the energy of the given final state of Ne^{++}. Atomic units are used throughout the paper unless specified otherwise. The energy ϵ_k or $\frac{1}{2}k^2$ was calculated both by evaluating the difference between Hartree-Fock calculations for E_i and E_f and also by including estimates of the difference in relativistic and correlation energies between E_i and E_f. The results are listed in Table I along with the experimental values of Körber and Mehlhorn.[17]

The Hartree-Fock results were obtained with a program generously provided by Fischer.[18] The relativistic corrections were estimated from the Dirac-Fock calculations on Ne by Desclaux[19] and

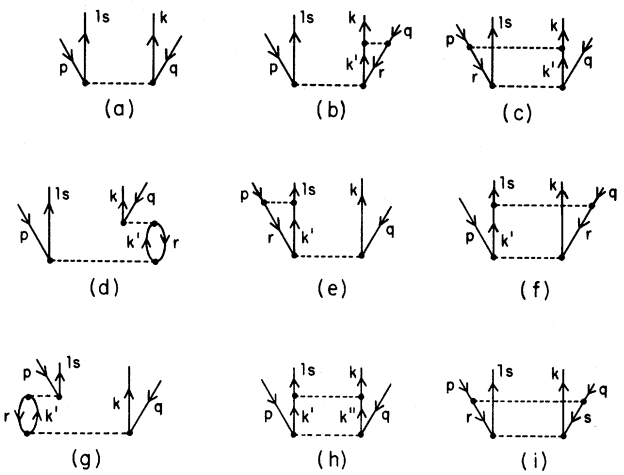

FIG. 1. Diagrams contributing to the Auger-rate matrix element. (a) lowest-order diagram; (b), (c), (d), and (i) are correlation correction diagrams equivalent to configuration mixing in the final state. Diagrams (e)–(h) involve correlations or configuration mixing in the initial state. Diagrams (d) and (e) also represent the diagrams obtained by including the exchange of the bottom matrix element.

the Lamb-shift calculations by Hartmann and Clementi.[20] The correlation energies were estimated from the results for pair correlations in Ne given by Viers, Harris, and Schaefer[21] and by Barr and Davidson.[22] The correlation energy of Ne^+ $1s2s^2 2p^6$ relative to that of Ne was taken from Ref. 15 as was the correlation energy involved in $2p \rightarrow 2s$ transitions when there is a $2s$ vacancy. The correlation energy involved in $2s \rightarrow 2p$ transitions when there is a $2p$ vacancy was estimated from previous work[23] on oxygen $(1s)^2(2s)^2(2p)^4$. However, the correlation energy associated with $2s^2 \rightarrow 2p^2$ and $2p^2 \rightarrow 2s^2$ transitions was calculated explicitly.

For the $1s2s^22p^6$ state of Ne^+, which we may denote as Ne^+ $(1s^{-1})$, we obtained the relativistic energy of the $1s$ orbital by considering the value of the one-electron integral I_{1s} as defined by Desclaux[19] which reduces in the nonrelativistic limit to the kinetic energy and interaction with the field of the nucleus. From Ref. 19, the relativistic contribution to I_{1s} is -0.0664 a.u. for Ne. Since this relativistic contribution is proportional to Z^4 and the $1s$ screening parameters for Ne and Ne^+ $1s2s^2 2p^6$ are 0.484 and 0.288, respectively, in our HF calculations, the $1s$ relativistic energy for Ne^+ $(1s^{-1})$ is approximately -0.072 a.u. The Lamb-shift contribution[20] is 0.0043 a.u. The relativistic shift for each $2s$ electron is approximately[19] -0.00545 a.u. The total relativistic energy for Ne as given by Desclaux,[19] excluding the Lamb shift, is -0.127 a.u. The total relativistic and Lamb-shift energy for Ne^+ $(1s^{-1})$ relative to Ne is then 0.0398 a.u. The correlation energy for Ne^+ $(1s^{-1})$ relative to Ne is 0.0298 a.u.,[15] and the difference in HF energies was calculated to be 31.92144 a.u. The resulting total difference in energy between Ne^+ $(1s^{-1})$ and Ne is then 31.9910 a.u. or 870.53 eV. This result is in good agreement with an experimental value of 870.2 eV reported by Siegbahn *et al.*[24] and a calculated value of 870.5 eV by Beck and Nicolaides.[25]

In calculating the energy of Ne^{++} $(1s)^2(2p)^6$ relative to Ne, the difference in HF energies is 4.47056 a.u. The correlation energy difference has contributions from the negative of all the pair correlations which are missing for $(1s)^2(2p)^6$ relative to Ne. That is, we consider the negative of the correlation energy for all the $2s$-$1s$, $2s$-$2s$, and $2s$-$2p$ pairs. From Refs. 21 and 22, we obtain 0.10123 a.u. There is also a contribution from $2p^2 \rightarrow 2s^2$ transitions which was calculated to be 0.07276 a.u. There are also other transitions with one $2p \rightarrow 2s$ transition and a $2p \rightarrow k$ transition, where k is an excited orbital. From Ref. 15, the correlation energy due to virtual transitions into a $2s$ hole state of Ne^+ including pair correlations and three-body correlations is -0.0791 a.u. Since there are now two $2s$ hole states, this contribution is -0.1582 a.u. From the $2s$ relativistic energy there is a shift of 0.01090 a.u. for $(1s)^2(2p)^6$ relative to Ne. The sum of all these effects is 4.49725 a.u. The difference in energy between Ne^+ $1s2s^22p^6$ and Ne^{++} $1s^22p^6$ is then 27.49375 a.u. or 748.15 eV.

The same methods were used in obtaining the energies of the remaining multiplets. When there is a $2p$ vacancy in the final state, there is a contribution to the correlation energy due to excitations into the $2p$ vacancy, mostly from $2s$ excitations. These contributions were estimated from our previous results on oxygen $(1s)^2(2s)^2(2p)^4$ in which such correlations were calculated. For the final configuration $(1s)^2(2s)^2(2p)^4$ these contributions were estimated as -0.0375 a.u. For the final-state $1s^22s^22p^4$ ^1S there is also a contribution of -0.07269 a.u. due to $2s^2 \rightarrow 2p^2$ excitations. Three-body effects for $1s^22s^22p^4$ ^1S when there is a $2s^2 \rightarrow 2p^2$ excitation were calculated as 0.0248 a.u. However, when using the pair correlation results from Refs. 21 and 22, we have omitted three-body and higher effects since the pair correlation energies of Ref. 21 and 22 are too low by approximately the amount of three-body contributions, and the pair correlation energies sum to give a good value for the total correlation energy. In calculating the correlation energy for $1s^22s^22p^4$ ^1S, the second-order energy cross terms between the three determinants of the ^1S state were explicitly calculated for $2p^2 \rightarrow kd\ k'd$ excitations.

The results of Table I and the $1s$ removal energy for Ne are in reasonable agreement with experiment. It is somewhat surprising that the HF results are so good, and this seems to be due to partial cancellations between relativistic and correlation energy contributions. Although it is possible to carry out accurate correlation energy calculations using the methods of Ref. 14, this would have been much more time consuming than the approximate methods used here; and the main

TABLE I. Energies of the K-LL Auger lines of Ne (in eV).

Line	Hartree-fock	CORR [a]	Experiment [b]
$1s$-$2s2s$ ^1S	746.99	748.15	748.0 ± 0.1
$1s$-$2s2p$ ^1P	770.86	771.71	771.4 ± 0.1
$1s$-$2s2p$ ^3P	783.01	782.45	782.0 ± 0.1
$1s$-$2p2p$ ^1S	800.97	801.27	800.4 ± 0.1
$1s$-$2p2p$ ^1D	806.04	804.51	804.15 ± 0.4

[a] Including estimates of relativistic and correlation energy corrections.

[b] From the experiment of Körber and Mehlhorn, Ref. 17.

purpose of this work is to calculate accurate Auger intensities.

B. $1s\text{-}2s2s\ ^1S$ Auger rate

We first consider the KL_1L_1 intensity; that is, the Auger rate to $(1s)^2(2p)^6\ ^1S$. This transition is also denoted $1s\text{-}2s2s\ ^1S$. The lowest-order contribution to the Auger matrix element of Fig. 1(a) is $\langle 1sk|v|2s2s\rangle$, where k is the continuum orbital. As discussed earlier, the $1s$ and k orbitals are chosen to be HF orbitals of the state $(1s)^2(2p)^6 ks\ ^2S$. The $2s$ orbital is a Hartree-Fock orbital of the initial state $1s(2s)^2(2p)^6\ ^2S$. In order to be even closer to the physical situation, spin-polarization effects were included by choosing the initial $1s$ orbital of $1s(2s)^2(2p)^6$ to be $1s^+$, that is, to have "spin up." Spin-polarized $2s^+$ and $2s^-$ orbitals were calculated with full exchange and no exchange with the $1s$ orbital, respectively. The lowest-order matrix element is then $\langle 1s\,k|v|\,2s^-2s^+\rangle$. Our continuum state normalization is [14]

$$P_{kl}(r)=\cos[kr+\delta_l+(q/k)\ln 2kr-\tfrac{1}{2}(l+1)\pi] \qquad (3)$$

as $r\to\infty$ with $V(r)\to q/r$. Using Eq. (3), the Auger rate is [15]

$$P_A=(4/k)|\langle\Psi_f|\Sigma v_{ij}|\Psi_i\rangle|^2, \qquad (4)$$

where $|\Psi_i\rangle$ and $|\Psi_f\rangle$ are initial and final states, respectively. The value for $\langle 1s\,k|v|\,2s^-2s^+\rangle$ was calculated to be 0.041967 a.u., with the state $|k\rangle$ orthogonalized to $|1s\rangle$ and $|2s\rangle$ of $1s(2s)^2(2p)^6$. Without this orthogonalization, the matrix element is 0.043539 a.u. The Hartree-Fock spin-polarized result was verified by starting with the matrix element $\langle 1sk|v|2s^+2s^+\rangle$ and using perturbation theory to include the effects of spin polarization. Using the matrix element $\langle 1sk|v|2s^-2s^+\rangle$, the KL_1K_1 Auger rate is 0.9508×10^{-3} a.u., which is in very poor agreement with the experimental value $(0.35\pm0.07)\times10^{-3}$ a.u. measured by Mehlhorn, Stalherm, and Verbeek.[10] For comparison, Walters and Bhalla[26] and McGuire[27] report values of 0.89×10^{-3} a.u. and 0.82×10^{-3} a.u., respectively, in Hartree-Slater calculations. If we use the matrix element $\langle 1sk|v|2s^+2s^+\rangle$, the Auger rate is improved to 0.760×10^{-3} a.u. However, the matrix element $\langle 1sk|v|2s^-2s^+\rangle$ is better justified on physical grounds even though it leads to worse agreement with experiment; and it is expected that correlation effects must be included if reasonable agreement with experiment is to be achieved.

The correlation effects were included by calculating diagrams (b) through (i) of Fig. 1 using the methods of Ref. 14. Diagram 1(i) with $p=2s^-$, $q=2s^+$, $r=2p^-$, and $s=2p^+$ corresponds to configuration mixing of the final states of Ne^{++} $(1s)^2(2p)^6\ ^1S$ and Ne^{++} $(1s)^2(2s)^2(2p)^4\ ^1S$ as considered previously by Asaad[7,8] for Z between 12 and 36 and by Bhalla[9] for Ne. The calculations by Bhalla only gave the ratios of intensities but did not give the absolute intensities due to this configuration mixing. In this work this effect was calculated both by evaluating diagram 1(i) and also by configuration mixing using HF orbitals. The results by each method are very close and a contribution of -0.005927 a.u. was obtained for the Auger matrix element. At this point the Auger rate is 0.70116×10^{-3} a.u., which is appreciably better than the HF result but is still in rather poor agreement with experiment. Diagrams (b) through (h) of Fig. 1 were then calculated and found to contribute significantly. The largest contribution by far came from the diagrams of Figs. 1(b), (c), and (d) with $p=2s^-$, $q=2s^+$, $k=ks$, $k'=k'p$, and $r=2p$, where ks and kp are continuum orbitals with $l=0$ and $l=1$, respectively. This effect corresponds to configuration mixing of the final state $(1s)^2(2p)^6 ks\ ^2S$ with the states $(1s)^2(2s)(2p)^5 kp\ ^2S$. Diagram 1(b) contributed -0.004537 a.u. and diagram 1(c) contributed -0.001508 a.u., the sum of these diagrams slightly exceeding the contributions from the configuration mixing of Ne^{++} $(1s)^2(2p)^6\ ^1S$ and $Ne^{++}\,1s^2\,2s^2\,2p^4\ ^1S$. Diagram 1(d) with $r=2p$ and its exchange contributed $+0.001725$ a.u. The sum of diagrams 1(e), (f), and (g) (with exchange) with $p=2s^-$, $q=2s^+$, and $r=2p$ is -0.001478 a.u. There are also contributions from diagrams (b), (d), (f), and (g) with $r=1s$ which totaled 0.000767 a.u. The ladder diagrams of Fig. 1(h) contributed -0.000948 a.u., the largest contribution coming from $k's$, $k''s$ intermediate states.

These results are summarized in Table II. Using the total in Table II, the KL_1L_1 Auger rate becomes 0.488×10^{-3} a.u., which is considerably improved over the HF value but is still outside of the limits reported by Mehlhorn *et al.*[10] The overlap correction factor was calculated to be 0.99078, and the normalization factor, which accounts for the fact that the correlated many-body state $|\Psi_i\rangle$ is not normalized,[14] was calculated to be 0.99095. These factors change the KL_1L_1 Auger rate to 0.479×10^{-3} a.u. When the remaining Auger rates were calculated the effects of higher-order terms on the KL_1L_1 matrix element were roughly estimated using geometrical approximation to be 0.000348 a.u. This leads to a final KL_1L_1 Auger rate of 0.4902×10^{-3} a.u., which is in a little worse agreement with experiment than if we had not estimated the higher-order terms beyond those of Fig. 1. It should be noted that although the final-state mixing between $(1s)^2(2p)^6\ ^1S$ and $(1s)^2(2s)^2(2p)^4\ ^1S$ is important, the remaining

diagrams of Fig. 1 are equally important, although more difficult to calculate. Contributions involving imaginary parts of the matrix elements were very small and are not listed.

C. $1s\text{-}2s2p\ ^1P$ Auger rate

In calculating the $KL_1L_2(^1P)$ or $1s\text{-}2s\,2p\ ^1P$ Auger rate in LS coupling, we evaluate the matrix element $\langle\Psi_f|\Sigma v_{ij}|\Psi_i\rangle$, where $|\Psi_f\rangle$ is the final state $(1s)^2(2s)(2p)^5\,^1P\,kp\,^2S$ and $|\Psi_i\rangle$ is the initial state $(1s)(2s)^2(2p)^6\,^2S$, and $v_{ij}=e^2/r_{ij}$. In the HF approximation, the matrix element $\langle\Psi_f(^1P)|\Sigma v_{ij}|\Psi_i\rangle$ for the ^1P transition is

$$\langle\Psi_f(^1P)|\Sigma v_{ij}|\Psi_i\rangle = \sqrt{\tfrac{3}{2}}(\langle 1skp|v|2s2p\rangle + \langle 1skp|v|2p2s\rangle), \quad (5)$$

where there is an angular factor of $\frac{1}{3}$ associated with the matrix element $\langle 1skp|v|2p2s\rangle$. The final-state kp orbital was calculated in the HF potential of the final state $|\Psi_f(^1P)\rangle$. The matrix elements $\langle 1skp|v|2s2p\rangle$ and $\langle 1skp|v|2p2s\rangle$ were calculated to be 0.035350 and 0.015166 a.u. respectively. The resulting HF Auger rate is 2.0334×10^{-3} a.u. as compared with the experimental result $(0.96\pm0.19)\times10^{-3}$ a.u. of Mehlhorn *et al.*[10] Again, the HF result is considerably higher than experiment and correlation effects must be examined.

In Table III are listed contributions to the various diagrams of Fig. 1. Using the total of Table I in place of $(\langle 1skp|v|2s2p\rangle + \langle 1skp|v|2p2s\rangle)$, the total calculated Auger rate is 1.396×10^{-3} a.u., which is in much better agreement with the experimental value than the Hartree-Fock value. However, the calculated value is still considerably higher than the experimental value although the calculated ratio of the ^1P and $1s\text{-}2s2s\ ^1S$ rate is 2.861 as compared with the experimental ratio[10] of 2.743. Estimates of higher-order terms were quite small. The overlap factor was calculated to be 0.992541 and the normalization correction was calculated to be 0.986708, giving a final ^1P rate equal to 1.373×10^{-3} a.u. From Table III, it is seen that the largest correlation contributions come from diagram 1(c) with $p=2s$, $q=2p$, $r=2p$, and $k'=kd$ and from diagram 1(b) with $p=2p$, $q=2s$, $r=2p$, and $k'=kd$. These diagrams are calculated by principal value integration, and represent configuration mixing between the configurations $(1s)^2(2s)(2p)^5\,^1P\,kp\,^2S$ and $(1s)^2(2s)^2(2p)^4\,^1D\,kd\,^2S$. It is not surprising that mixing with this configuration is important since the Auger rate to the final-state $(1s)^2(2s)^2(2p)^4\,^1D$ is considerably larger than any other. As shown in Table III, there is much cancellation among the remaining correlation contributions. Those few contributions not explicitly listed in Table III are either identically zero or were estimated to be very small.

D. $1s\text{-}2s2p\ ^3P$ Auger rate

For the Auger transition to the final state, $(1s)^2(2s)(2p)^5\,^3P\,kp\,^2S$, the lowest-order Auger matrix element is

$$\langle\Psi_f(^3P)|\sum_{i<j} v_{ij}|\Psi_i\rangle = (3/\sqrt{2})(\langle 1skp|v|2s2p\rangle - \langle 1skp|v|2p2s\rangle), \quad (6)$$

where the matrix element $\langle 1skp|v|2p2s\rangle$ has an angular factor of $\frac{1}{3}$. It is noted from Eq. (6) that the diagram of Fig. 1(a) with $p=2p$, $q=2s$ is positive when projected onto $\Psi_f(^3P)$ but diagram 1(a) with $p=2p$ is negative when projected onto $\Psi_f(^3P)$.

From Table III, $\langle 1skp|v|2s2p\rangle$ is 0.034765 a.u. and $-\langle 1skp|v|2p2s\rangle$ is -0.016538 a.u. The lowest-order value for the $KL_1L_3\ ^3P$ or $1s\text{-}2s2p\ ^3P$ Auger rate is then 0.7888×10^{-3} a.u. as compared with the measured value[10] of $(0.35\pm0.07)\times10^{-3}$ a.u. When the correlations of Table III are included, the $1s\text{-}2s2p\ ^3P$ Auger rate becomes 0.5015×10^{-3} a.u., which is in better agreement with experiment although still too large to be within the quoted experimental accuracy. It is interesting to note that many of the diagrams contributing strongly in the ^1P case cancel exactly in the ^3P case. For example, diagram (c) with $p=2p$, $q=2s$, $r=2p$, and $k'=kd$ and diagrams (b) with $p=2p$, $q=2s$, $r=2p$, and $k'=kd$ provided the largest correlation effects in the ^1P case. For the ^3P intensity, these same diagrams are individually large numerically but

TABLE II. Contributions to the $1s\text{-}2s2s\ ^1S$ Auger matrix element.

Diagram of Fig. 1[a]	Value in a.u.
(a) $k=ks$	0.041 967
(b) $r=2p$	−0.004 537
(c) $r=2p$	−0.001 508
(d) $r=2p$	0.001 725[b]
(e) $r=2p$	−0.000 714
(f) $r=2p$	−0.000 114
(g) $r=2p$	−0.000 650
(b) $r=1s$	0.002 350
(d) $r=1s$	−0.001 966
(f) $r=1s$	0.000 360
(g) $r=1s$	0.000 024
(h)	−0.000 948
(i) $r=2p$, $s=2p$	−0.005 927
Total	0.030 062

[a] In all diagrams $p=2s^-$ and $q=2s^+$. All integrations over singularities were by principal-value integration.

[b] Exchange diagram with bottom matrix element equal to $\langle k\ 1s\ |v|\ pr\rangle$ included.

cancel. For the ^3P case, since diagrams (a) with $p=2s$, $q=2p$, and $p=2p$, $q=2s$ are of opposite sign the ^3P matrix element as given in Table III is much smaller than the ^1P matrix element. [It should be noted that the entries in Table III do not contain the angular factors $\sqrt{\frac{3}{2}}$ and $3/\sqrt{2}$ given in Eqs. (5) and (6).] For the ^3P case, the ladder diagrams of Fig. 1(h) are of greater importance than for ^1P. Also, the diagrams with a $1s$ hole line [i.e., diagrams (b) and (d) with $r=1s$] are not important for ^1P transitions but are significant in the ^3P case. For ^3P relative to ^1P, note that diagram (b) with $p=2p$, $q=2s$, $r=1s$ is considerably reduced. This is because in the ^3P case only $\frac{1}{3}$ of the Coulomb matrix elements have $q=2s^+$ but $r=1s^+$ always.

E. $1s$-$2p2p$ ^1S Auger rate

The next rate to be calculated is KL_2L_2 ^1S or $1s$-$2p2p$ ^1S, where the final state is $\Psi_f(^1S)$ $=(1s)^2(2s)^2(2p)^4$ ^1S ks ^2S. The Auger matrix element in LS coupling is

$$\langle \Psi_f(^1S)| \sum_{i<j} v_{ij} |\Psi_i\rangle = (3)^{-1/2}\langle 1s\ ks\ |v|\ 2p2p\rangle_R , \tag{7}$$

where $\langle 1s\ ks\ |v|\ 2p2p\rangle_R$ is the radial part of $\langle 1s\ ks\ |v|\ 2p2p\rangle$ or $R^1(1s\ ks,\ 2p2p)$ in the notation of Condon and Shortley.[28] The calculated value for $R^1(1s\ ks,\ 2p2p)$ is -0.051214 which leads to an Auger rate 0.45596×10^{-3} a.u. as compared to the measured rate of $(0.55\pm0.11)\times10^{-3}$ a.u. of Mehlhorn *et al.*[10]

As discussed already in connection with the $1s$-$2s2s$ ^1S rate, there is considerable configuration mixing between the final states of Ne^{++} $(1s)^2(2p)^6$ ^1S and $(1s)^2(2s)^2(2p)^4$ ^1S. The lowest-order diagram contributing to this rate is Fig. 1(i)

TABLE III. Contributions to the $1s$-$2s2p$ ^1P and $1s$-$2s2p$ ^3P Auger matrix elements (in a.u.).

Diagram of Fig. 1[a]		$1s$-$2s2p$ ^1P	$1s$-$2s2p$ ^3P
$p=2s$, $q=2p$	(a)	0.035 350	0.034 765
	(b) $r=2s$	0.001 589	0.000 529
	(c) $r=2p$, $k'=kd$	−0.004 461	−0.002 875
	(c) $r=2p$, $k'=ks$	−0.000 234	0.000 000[b]
	(d) $r=2s$, $k'=ks$	0.000 006	0.000 009
	(e) $r=2p$, $k'=kp$	−0.000 431	0.000 000[d]
	(f) $r=2s$, $k'=kp$	−0.000 005	−0.000 000[e]
	(f) $r=2p$, $k'=kskd$	0.000 019	0.000 018
	(g) $r=2p$, $k'=kp$	−0.000 533	−0.000 544
	(g) $r=2s$, $k=k's$	−0.000 096	−0.000 095
	(h)	−0.001 503	−0.001 503
	(b) $r=1s$, $k'=ks$	−0.000 067	−0.000 076
	(d) $r=1s$, $k'=ks$	−0.001 366	−0.001 349
$p=2p$, $q=2s$	(a)	0.015 166	−0.016 538[c]
	(b) $r=2p$, $k'=kd$	−0.004 461	0.002 875
	(b) $r=2p$, $k'=ks$	−0.000 234	0.000 000[b]
	(c) $r=2s$, $k'=ks$	0.001 589	−0.000 529
	(d) $r=2p$, $k'=kd$	0.000 845	−0.000 702
	(d) $r=2p$, $k'=ks$	0.000 049	−0.000 049
	(e) $r=2k$, $k'=kd$	0.000 057	−0.000 056
	(e) $r=2p$, $k'=ks$	−0.000 007	0.000 007
	(e) $r=2s$, $k'=kp$	−0.000 005	0.000 000[e]
	(f) $r=2p$, $k'=kp$	−0.000 141	0.000 000[d]
	(g) $r=2p$, $k'=kd$	−0.000 319	0.000 312
	(g) $r=2s$, $k'=kp$	−0.000 026	0.000 017
	(h)	−0.000 382	0.000 382
	(b) $r=1s$, $k'=kp$	0.002 090	−0.000 702
	(d) $r=1s$, $k'=kp$	−0.000 639	0.000 638
Total		0.041 850	0.014 534

[a] The angular factors $\sqrt{\frac{3}{2}}$ and $3/\sqrt{2}$ for the ^1P and ^3P cases, respectively, are not included in the numbers listed.

[b] Not calculated since (c) with $p=2s$, $q=2p$ cancels (b) with $p=2p$, $q=2s$.

[c] Note minus sign in this and all following matrix elements of this column when projection of diagram is made onto $(1s)^2(2s)(2p)^5$ ^3P kp ^2S final state.

[d] Not calculated since (e) with $p=2s$, $q=2p$ cancels (f) with $p=2p$, $q=2s$.

[e] Not calculated since (f) with $p=2s$, $q=2p$ cancels (e) with $p=2p$, $q=2s$.

with $p=2p^-$, $q=2p^+$, $r=2s^-$, $s=2s^+$. The results are very nearly the same whether we calculate Fig. 1(i) or diagonalize the configuration interaction (CI) matrix. The CI result adds -0.012545 a.u. to R^1 $(1s\,ks,\ 2p2p)$ and leads to the Auger rate 0.7067×10^{-3} a.u. Although this result is higher than experiment, the ratio to the correlated $1s2s2s\ ^1S$ rate is 1.45 which is in resonable agreement with the experimental[10] ratio of 1.57.

There is no justification, however, for not including all the correlation diagrams of Fig. 1. These are listed in Table IV. Diagrams (b) and (c) with $r=2p$ and $k'=kd$ are large. This, again, is expected since these diagrams account for configuration mixing of $(1s)^2(2s)^2(2p)^4\ ^1S\ ks\ ^2S$ with $(1s)^2(2s)^2(2p)^4\ ^1D\ kd\ ^2S$, and the ^1D Auger rate is the largest rate by far. Diagrams (b) and (c) with $r=2s$, $k'=kp$ are also significant and represent configuration mixing of $(1s)^2(2s)^2(2p)^4\ ^1S\ ks\ ^2S$ with $(1s)^2(2s)(2p)^5\ ^{3,1}P\ kp\ ^2S$. The effects of correlation in the initial-state $1s(2s)^2(2p)^6\ ^2S$ are represented by diagram (h) and these are seen to be also important. The largest effect is contributed by diagram (i) which accounts for configuration mixing of $(1s)^2(2s)^2(2p)^4\ ^1S\ ks\ ^2S$ and $(1s)^2(2p)^6\ ^1S\ ks\ ^2S$ as already discussed. Using the total of Table IV and the fact that $k=7.6699$ a.u., the resulting Auger rate is 0.8618×10^{-3} a.u. For this case, the effect of a spin polarization correction has also been investigated; that is, $2p^{\pm}$ orbitals were calculated with no exchange with the 1s orbital $(2p^-)$ and full exchange with the 1s orbital $(2p^+)$. The change in the basic matrix element $\langle 1sks|v|2p^-2p^+\rangle$ is -0.000102. The Auger rate then becomes 0.8643×10^{-3} a.u., which is considerably higher than the experimental value[10] of $(0.55\pm0.11)\times10^{-3}$ a.u. The ratio to the corresponding $KL_1L_1(^1S)$ rate is, however, 1.77, which is in reasonable agreement with the experimental[10] ratio of 1.57. An estimate has been made of higher-order terms for this Auger rate. Since diagram (i) (or the corresponding configuration mixing effect) gives the largest correlation contribution for this rate it seems desirable desirable to examine corrections to this term. These are easily included by replacing $\langle 1sks|v|2s2s\rangle$ of diagram (i) by the correlated matrix element obtained from Table II excluding the correlations due to mixing with $(1s)^2(2s)^2(2p)^4\ ^1S\ ks\ ^2S$. Diagram (i) is then reduced by the ratio 0.03599/0.04197. The higher-order modifications of diagram (i) then contribute 0.001787 a.u.

In a similar way, the modifications of the remaining diagrams which involve configuration mixing with $(1s)^2(2s)(2p)^5\ ^{1,3}P\ kp\ ^2S$ were estimated to contribute 0.001049 a.u. Modifications of diagrams involving configuration mixing with $(1s)^2(2s)^2(2p)^4\ ^1D\ kd\ ^2S$ were estimated in this same way as only 0.000243 a.u. due to the small effects of correlations on the ^1D rate, which will be discussed. Including these effects, the $KL_1L_2\ (^1S)$ Auger rate becomes 0.7904×10^{-3} a.u. Including the overlap factor of 0.9937 and the normalization factor of 0.98128, the $KL_2L_2(^1S)$ Auger rate becomes 0.7707×10^{-3} a.u. Although this result is larger than experiment,[10] the ratio to the $KL_1L_1(^1S)$ rate is 1.572, which is in good agreement with the ratio of experimental values.

F. $1s$-$2p2p\ ^1D$ Auger rate

The final Auger rate to be calculated is the transition to the final state, $\Psi_f(^1D)=(1s)^2(2s)^2(2p)^4\ ^1D\ kd\ ^2S$. The Auger matrix element

$$\langle\Psi_f(^1D)|\sum_{i<j}v_{ij}|\Psi_i\rangle=-\sqrt{\tfrac{2}{3}}\,\langle 1s\ kd\ |v|\ 2p2p\rangle_R\,, \quad (8)$$

where $\langle 1s\ kd\ |v|\ 2p2p\rangle_R$ is the radial part of the matrix element, or R^1 $(1s\ kd,\ 2p2p)$. The calculated value for $\langle 1s\ kd\ |v|\ 2p2p\rangle_R$ is 0.128021 a.u. and the value for k is 7.687871 a.u., resulting in an Auger rate of 5.685×10^{-3} a.u. as compared with the experimental value[10] of $(3.28\pm0.066)\times10^{-3}$ a.u. Contributions to the diagrams of Fig. 1 are listed in Table V. Certain diagrams are cancelled, of course, by the HF potential. The largest contributions are from diagram (c) with $r=2s$ and $k'=kp$

TABLE IV. Contributions to the $KL_2L_2(^1S)$ Auger matrix elements (in a.u.).

Diagram of Fig. 1 [a]	Value [b]
(a)	−0.051 214
(b) + (c) $r=2p$, $k'=kd$	−0.006 147
(b) $r=2s$, $k'=kp$	−0.001 515
(c) $r=2s$, $k'=kp$	−0.003 938
(d) $r=2p$, $k'=kd$	0.000 268
(d) $r=2s$, $k'=kp$	−0.000 183
(e) + (f) $r=2p$, $k'=kd$	−0.000 233
(e) $r=2s$, $k'=kp$	−0.000 097
(f) $r=2s$, $k'=kp$	−0.000 418
(g) $r=2p$, $k'=kd$	0.000 258
(g) $r=2s$, $k'=kp$	0.000 038
(b) $r=1s$, $k'=kp$	−0.002 397
(d) $r=1s$, $k'=kp$	0.002 201
(g) $r=1s$, $k'=kp$	0.000 688
(h) $k'=k's$, $k''=k''s$	−0.002 175
(h) $k'=k'p$, $k''=k''p$	0.005 980
(h) $k'=k'd$, $k''=k''d$	0.001 021
(i) $r=2s$, $s=2s$	−0.012 545
Total	−0.070 408

[a] $p=2p$, $q=2p$ in all diagrams; $k=ks$ for $1s$-$2p2p\ ^1S$ case. Bound and continuum states are included in the sum over excited states. Results for (d) and (g) include exchange in bottom matrix element.

[b] The angular factor of $\frac{1}{3}$ from the diagram of Fig. 1(a) has been factored out of all contributions.

and from diagram (h). The contribution from diagram (c) with $r = 2s$ represents final-state configuration mixing with $(1s)^2(2s)(2p)^5\ ^{1,3}P\ kp\ ^2S$. Diagram (h) represents correlations in the initial state, and excited states k', k'' with $l = 0$, 1, 2, and 3 were included. Of these, the largest contribution by far is from $k' = k'p$, $k'' = k''p$, giving -0.008786 a.u. Using the correlated matrix element of Table V, the ^1D rate is 5.213×10^{-3} a.u. The change due to spin polarization corrections was calculated to be -0.000172 a.u., leading to a ^1D rate 5.198×10^{-3} a.u. Contributions from the imaginary parts of diagrams (b)–(d) were calculated and found to be very small.

Effects of higher-order diagrams were also estimated by multiplying the diagram of Fig. 1(c) by the ratio of the correlated to lowest-order ^1P matrix elements as given in Table III. The result is -0.001073 a.u. Contributions from higher-order diagrams but with three Coulomb interactions and both denominators giving imaginary parts were -0.000568 a.u. Including these effects, the ^1D rate becomes 5.060×10^{-3} a.u. Including a factor 0.9753 due to overlap and normalization effects, the final ^1D Auger rate is 4.935×10^{-3} a.u., which is still appreciably higher than the experimental value.[10]

The results of all calculated rates are summarized in Table VI and compared with experiment. The best calculated value for the total rate is 8.055×10^{-3} a.u. as compared with the experimental value $(5.49 \pm 0.51) \times 10^{-3}$ a.u. This may be compared with the values 10.0×10^{-3} a.u. calculated by Walters and Bhalla[26] in a Hartree-Fock-Slater calculation and 9.48×10^{-3} a.u. calculated by McGuire[27] in an approximate Hartree-Fock-Slater calculation. It is interesting to note that the Hartree-Fock-Slater results are in close agreement with the Hartree-Fock result 9.914×10^{-3} a.u. of Table VI. Including correlations affects many of the individual rates much more than it does the total Auger rate. This is because the largest single rate is the $1s$-$2p2p\ ^1D$ rate, which is least affected by inclusion of correlation terms. Many of the important correlation terms affecting the other rates come from configuration mixing with the $(1s)^2(2s)^2(2p)^4\ ^1D\ kd\ ^2S$ states.

The results listed under CORR I and CORR II in Table VI are generally in much better agreement with the experiment than the Hartree-Fock values. Although the correlated results are outside experimental error, they are consistently high. The ratios of the CORR II rates to experiment range from 1.40 for the $KL_1L_1(^1S)$ rate to 1.51 for the ^1D rate. The ratios of the rates relative to the $KL_1L_1(^1S)$ rate have been measured in several experiments[11,17,29] and have also been calculated by Bhalla.[9] Ratios of intensities relative to $KL_1L_1(^1S)$ are listed in Table VII. The best calculated values are those labeled CORR II, and these ratios are in good agreement with experiment.

TABLE V. Contributions to the $1s$-$2p\,2p\ ^1D$ Auger matrix elements (in a.u.).

Diagram of Fig. 1[a]	Value[b]
(a)	0.128 021
(b) $r = 2p$, $k' = ks$	−0.000 860
(b) $r = 2s$, $k' = kp$	0.002 227
(c) $r = 2p$, $k' = ks$	−0.000 860
(c) $r = 2s$, $k' = kp$	0.006 256
(d) $r = 2p$, $k' = ks$	0.000 362
(d) $r = 2s$, $k' = kp$	0.000 374
(e) $r = 2p$, $k' = kd$	0.000 354
(e) $r = 2s$, $k' = kp$	0.000 186
(f) $r = 2p$, $k' = kd$	0.000 126
(f) $r = 2s$, $k' = kp$	−0.000 706
(g) $r = 2p$, $k' = kd$	−0.001 400
(g) $r = 2p$, $k' = ks$	−0.000 000
(g) $r = 2s$, $k' = kp$	−0.000 230
(h)	−0.010 343
(b) $r = 1s$, $k = k'p$	0.004 233
(d) $r = 1s$, $k = k'p$	−0.004 570
(g) $r = 1s$, $k = k'p$	−0.000 579
Total	0.122 591

[a] $p = 2p$, $q = 2p$, and $k = kd$ in all diagrams. Results for (d) and (g) include exchange in bottom matrix element. Bound and continuum states are included in the sum over excited states.

[b] The angular factor for diagram (a) has been factored out of all contributions.

TABLE VI. Auger rates for Ne $(1s^{-1})$.[a]

Transition[b]	HF[c]	CORR I[d]	CORR II[e]	Expt[f]
$1s$-$2s2s\ (^1S)$	0.9508	0.4879	0.4902	0.35 ± 0.07
		0.7012[g]		
$1s$-$2s2p\ (^1P)$	2.0335	1.3956	1.3670	0.96 ± 0.19
$1s$-$2s2p\ (^3P)$	0.7888	0.5015	0.4922	0.35 ± 0.07
$1s$-$2p2p\ (^1S)$	0.4560	0.8643	0.7707	0.55 ± 0.11
		0.7067[g]		
$1s$-$2p2p\ (^1D)$	5.6849	5.1983	4.9349	3.28 ± 0.066
Total	9.9140	8.4476	8.0550	5.49 ± 0.51

[a] All results given in units of 10^{-3} a.u.

[b] See text for notation.

[c] Hartree-Fock or lowest-order result.

[d] Including correlation diagrams of Fig. 1.

[e] Including correlation diagrams in Fig. 1, any estimates of higher-order diagrams as described in text, and small contributions from overlap and normalization factors as described in text.

[f] Experimental values from Ref. 10.

[g] Correlation effects only from mixing of $(1s)^2(2s)^2(2p)^4\ ^1S$ and $(1s)^2(2p)^6\ ^1S$.

TABLE VII. Ratios of Auger rates to the $1s$-$2s2s$ (^1S) rate.

Method	$1s$-$2s2p$ (^1P)	$1s$-$2s2p$ (^3P)	$1s$-$2p2p$ (^1S)	$1s$-$2p2p$ (^1D)
HF[a]	2.139	0.830	0.480	5.979
CORR II[b]	2.789	1.004	1.572	10.067
Bhalla[c]	2.98	0.99	0.99	8.3
Expt I[d]	3.06±0.07	0.98±0.05	1.67±0.08	13.1±0.6
Expt II[e]	2.73±0.04	1.00±0.02	1.55±0.03	9.31±0.15
Expt III[f]	2.87±0.05	1.06±0.05	1.5±0.1	10.00±0.18
Expt IV[g]	2.92±0.06	1.06±0.05	1.5±0.1	10.13±0.24

[a] Hartree-Fock calculation, this paper.

[b] Including correlation effects, this paper.

[c] Calculations by Bhalla, Ref. 9, including configuration mixing between Ne^{++} states $(1s)^2(2s)^2(2p)^4\,{}^1S$ and $(1s)^2(2p)^6\,{}^1S$.

[d] Ratios measured by Körber and Mehlhorn Ref. 17.

[e] Ratios measured by Stalherm, Ref. 29.

[f] Ratios measured by Krause *et al.*, Ref. 11, with initial vacancy created by electron impact of 3 to 10 keV.

[g] Ratios measured by Krause *et al.* Ref. 11, with initial vacancy created by 1.5-keV x rays.

IV. CONCLUSIONS

In this work it has been shown that the Hartree-Fock results for Auger transition rates are considerably improved when correlation effects are included. Although the configuration mixing of Ne^{++} $(1s)^2(2s)^2(2p)^4\,{}^1S$ and $(1s)^2(2p)^6\,{}^1S$ is important, good results can only be obtained by also considering the other correlation effects. The present calculations give intensity ratios in good agreement with experiment. However, the calculated absolute Auger rates are larger than experiment by factors ranging from 1.4 to 1.5, which is outside experimental error. It is not clear where the source of error lies, since estimates of higher-order diagrams involving correlation interactions of the types shown in Figs. 1(b)–(i) did not produce close agreement with experiment. One possible improvement would be to include the correlation effects on single-particle orbitals either by calculating the appropriate higher-order diagrams or by calculating the orbitals with an optical potential.[30] A practical approach might be to use the polarized orbitals method of Temkin.[31] These effects will be investigated in future work.

Note added in proof. Professor W. Mehlhorn and Dr. M. Krause have kindly brought to my attention the recent paper by U. Gelius, S. Svensson, H. Siegbahn, E. Basilier, A. Faxalv, and K. Siegbahn [Chem. Phys. Lett. 28, 1 (1974)] in which the width of the Ne $1s$ line is measured to be 0.23±0.02 eV or $(8.45\pm0.07)\times10^{-3}$ a.u., which is in good agreement with the results in Table VI.

ACKNOWLEDGMENTS

I wish to thank B. Crasemann, P. Fishbane, D. Matthews, and J. Trefil for helpful discussions. Also, I want to thank Dr. C. Froese Fischer for the use of her Hartree-Fock program.

*Work supported by the NSF.

[1] D. L. Matthews, B. M. Johnson, J. J. Mackey, and C. F. Moore, Phys. Rev. Lett. 31, 1331 (1973).

[2] D. Burch, N. Stolterfoht, D. Schneider, H. Wieman, and J. S. Risley, Phys. Rev. Lett. 32, 1151 (1974).

[3] R. L. Kauffman, F. Hopkins, C. W. Woods, and P. Richard, Phys. Rev. Lett. 31, 621 (1973).

[4] C. P. Bhalla and M. Hein, Phys. Rev. Lett. 30, 39 (1973).

[5] C. P. Bhalla, N. O. Folland, and M. A. Hein, Phys. Rev. A 8, 649 (1973).

[6] W. Bambynek, B. Crasemann, R. W. Fink, H. U. Freund, H. Mark, C. D. Swift, R. E. Price, and P. V. Rao, Rev. Mod. Phys. 44, 716 (1972).

[7] E. H. S. Burhop and W. N. Asaad, Adv. At. Mol. Phys. 8, 163 (1972).

[8] W. N. Asaad, Nucl. Phys. 66, 494 (1965).

[9] C. P. Bhalla, Phys. Lett. A 44, 103 (1973).

[10] W. Mehlhorn, D. Stalherm, and H. Verbeek, Z. Naturforsch. A 23, 287 (1968).

[11] M. O. Krause, F. A. Stevie, L. J. Lewis, T. A. Carlson, and W. E. Moddeman, Phys. Lett. A 31, 81 (1970).

[12] K. A. Brueckner, *The Many Body Problem* (Wiley, New York, 1959).

[13] J. Goldstone, Proc. R. Soc. A 239, 267 (1957).

[14] H. P. Kelly, Adv. Chem. Phys. 14, 129 (1969).

[15]R. L. Chase, H. P. Kelly, and H. S. Köhler, Phys. Rev. A 3, 1550 (1971).
[16]H. P. Kelly and A. Ron, Phys. Rev. A 5, 168 (1972).
[17]H. Körber and W. Mehlhorn, Z. Phys. 191, 217 (1966).
[18]C. Froese Fischer, Comput. Phys. Commun. 1, 151 (1969).
[19]J. P. Desclaux, At. Data Nucl. Data Tables 12, 311 (1973).
[20]H. Hartmann and E. Clementi, Phys. Rev. 133, A1295 (1964).
[21]J. W. Viers, F. E. Harris, and H. F. Schaefer III, Phys. Rev. A 1, 24 (1970).
[22]T. L. Barr and E. R. Davidson, Phys. Rev. A 1, 644 (1970).
[23]H. P. Kelly, Phys. Rev. 144, 39 (1966).
[24]K. Siegbahn, C. Nordling, G. Johansson, J. Hedman, P. F. Hedén, K. Hamrin, U. Gelius, T. Bergmark, L. O. Werme, R. Manne, and Y. Baer, *ESCA Applied to Free Molecules* (North-Holland, Amsterdam, 1969).
[25]D. R. Beck and C. A. Nicolaides, Chem. Phys. Lett. 27, 269 (1974).
[26]D. L. Walters and C. P. Bhalla, Phys. Rev. A 3, 519 (1971).
[27]E. J. McGuire, Phys. Rev. A 2, 273 (1970).
[28]E. U. Condon and G. H. Shortley, *The Theory of Atomic Spectra* (Cambridge U. P., Cambridge, England, 1957), p. 175.
[29]D. Stalherm, Diplomarbeit Inst. Kernphysik, Univ. Münster, 1968 (unpublished).
[30]A. L. Fetter and K. M. Watson, *Advances in Theoretical Physics* (Academic, New York, 1965), p. 115.
[31]A. Temkin, Phys. Rev. 107, 1004 (1957); R. J. Drachman and A. Temkin, *Case Studies in Atomic Collisions II* (North-Holland, Amsterdam, 1972), p. 399.